Composites: Part B 42 (2011) 2093–2097

Contents lists available at ScienceDirect

Composites: Part B

journal homepage: www.elsevier.com/locate/compositesb

Some issues on nanoindentation method to measure the elastic modulus of particles in composites

Wenyi Yan [a,*], Chung Lun Pun [a], Zonghui Wu [a], George P. Simon [b]

[a] Department of Mechanical & Aerospace Engineering, Monash University, Clayton VIC 3800, Australia
[b] Department of Materials Engineering, Monash University, Clayton VIC 3800, Australia

ARTICLE INFO

Article history:
Received 4 December 2010
Received in revised form 7 February 2011
Accepted 9 February 2011
Available online 9 May 2011

Keywords:
A. Particle-reinforcement
B. Mechanical properties
C. Computational modelling
Nanoindentation

ABSTRACT

The application of the indentation method to measure the elastic modulus of particles embedded in a composite is theoretically investigated in this paper by finite element simulation. The Oliver–Pharr method, which is widely used in commercial nanoindentation instruments, is used to probe the elastic modulus of the particle from the simulated indentation curve. The predicted elastic modulus is then compared with the inputted value. Two cases are studied, that of a stiff particle embedded in a soft matrix and a soft particle embedded in a stiff matrix. In both of these cases, there exists a particle-dominated depth. If the indentation depth lies within this particle-dominated depth, the Oliver–Pharr method is able to be applied to measure the particle's elastic modulus with sufficient accuracy if the real contact area is used. This could lead to an experimentally-convenient method of determining the primary properties of individual particle, providing they can be well dispersed in the polymeric matrix.

1. Introduction

In an instrumented indentation test, the so called nanoindentation test, a diamond indenter is pressed into the surface of a specimen to depths ranging from nanometers to micrometers. The curve of the indentation force versus the indentation depth is recorded, and used to extract the specimen's mechanical properties, such as elastic modulus and hardness. Due to its simplicity, convenience and the increasing availability of commercial nanoindentation instruments, such as Hysitron Triolab™ and MTS Nano Indenter® system, the nanoindentation test becomes a popular experimental method to probe the mechanical properties of different materials [1–6]. With regards characterization of nanomaterials and nanostructured materials, studies have looked at the mechanical properties of graphite flakes and spherulites in cast iron [7], AlN nanoparticle-reinforced nanocrystalline Al matrix composites [8], carbon nanotube/nanofiber-reinforced polymer composite [9] and graphene reinforced polymer composites [10].

The theory for using instrumented nanoindentation to probe the elastic modulus was developed by Oliver and Pharr in 1992 [11]. However, the Oliver–Pharr method is only suitable for monolithic and isotropic materials. When it is applied to nanocomposites, the measured elastic modulus is a function of the elastic properties of both the nanoparticle and the matrix. In particular, the influence of the matrix should be understood in order to understand and use the measured data. Additionally, the method described by Oliver–Pharr to predict the projected contact area, a prerequisite step to determine the elastic modulus and hardness, is only suitable for the indentations which display the deformation phenomenon of "sink-in", where the surface around the indenter sinks in. If the opposite indentation deformation phenomenon of "pile-up" occurs (the surface of the sample around the indenter being at a greater level than its surrounds), the elastic modulus and hardness can be significantly underestimated [12]. In this paper, an indentation of a particle embedded in a matrix is numerically simulated by the finite element method. The Oliver–Pharr method is then applied to probe the elastic modulus of the particle from the simulated indentation force versus indentation depth curve. The objective of the study is to investigate if the Oliver–Pharr method can be applied directly to measure the elastic modulus of the particles in a composite.

2. Methodology

2.1. Investigation model

A composite material system of particles embedded in a matrix was chosen in this research and is similar in morphology to many new particle reinforced composites [7–10]. For the reason of simplicity, an idealised semi-spherical particle embedded in the surface of a semi-infinite matrix is considered in this work, as shown in Fig. 1. A conical indenter with 70.3° was pressed at the centre of the semi-spherical particle. This configuration is equivalent to a

* Corresponding author. Tel.: +61 3 99020113; fax: +61 3 99051825.
E-mail address: wenyi.yan@monash.edu (W. Yan).

1359-8368/$ - see front matter © 2011 Elsevier Ltd. All rights reserved.
doi:10.1016/j.compositesb.2011.05.002

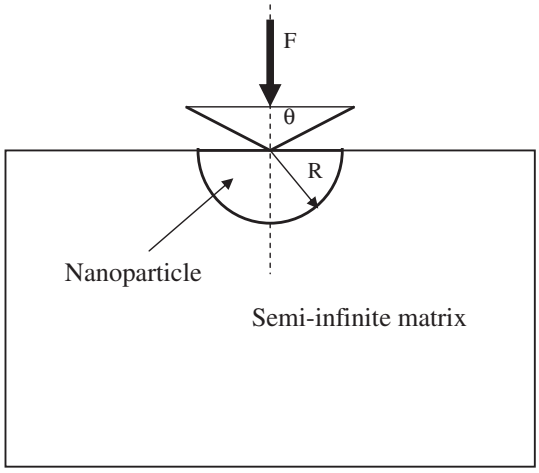

Fig. 1. Schematic illustration of the theoretical indentation model.

sharp Vickers or Berkovich indenter [13], which is commonly used in commercial indentation instruments.

The illustrated indentation in Fig. 1 was simulated in a virtual fashion by using an axisymmetric finite element model, see Fig. 2. The commercial finite element package Abaqus was utilised for the simulations. As demonstrated in Fig. 2b, a very fine mesh was employed in the contact zone beneath the indenter tip to ensure the accuracy of the numerical results. The model contains a total of 7997 four-noded, axisymmetric elements. The output indentation force versus the indentation depth curve was then used to predict the elastic modulus of the particle by strictly following the Oliver–Pharr method, which duplicated the procedure conducted by a nanoindenation instrument in a real, physical test. For this purpose, the Oliver–Pharr method is first briefly discussed below.

2.2. Oliver–Pharr method

The Oliver–Pharr method is the most common method for establishing the projected contact area and predicting the elastic modulus of ordinarily materials. This method begins by fitting the unloading portion of the indentation graph data to the power–law relation as below [11,14],

$$F = B(h - h_f)^m \tag{1}$$

where B and m are fitting parameters and h_f is the final indentation depth after complete unloading. From this data the initial unloading slope, i.e., contact stiffness, S, can be estimated by analytically differentiating Eq. (1) and evaluating the result at the maximum indentation depth, i.e.,

$$S = \left(\frac{dF}{dh}\right)_{h=h_{\max}} = Bm(h_{\max} - h_f)^{m-1} \tag{2}$$

The obtained contact stiffness from Eq. (2) is then used to estimate the contact depth h_c under the maximum indentation force,

$$h_c = h_{\max} - \varepsilon\frac{F_{\max}}{S} \tag{3}$$

where ε is a constant which depends on the indenter geometry. For conical indenters, ε has been suggested to be 0.72 [14]. The projected contact area, A, under the maximum indentation force for a sharp conical indenter is determined by the indenter tip's included angle, θ, which is 70.3° in our study and the estimated contact depth h_c from Eq. (3), that is,

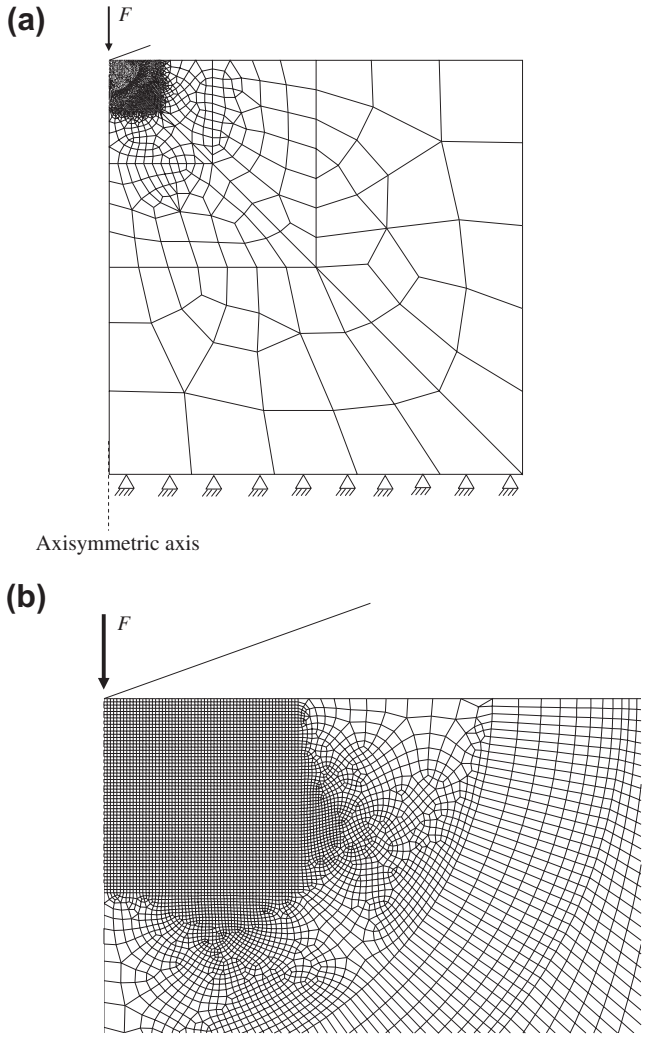

Fig. 2. Axisymmetric finite element model to simulate the indentation test with a rigid conical indenter: (a) entire finite element mesh and boundary conditions; (b) fine mesh near the indenter tip.

$$A = \pi(h_c \tan\theta)^2 \tag{4}$$

Finally, in the case of a rigid indenter, as assumed here, the elastic modulus of the particle, E_p^m, can be calculated by:

$$E_p^m = \frac{1}{\beta}\frac{\sqrt{\pi}}{2}\frac{S}{\sqrt{A}}(1 - \upsilon_p^2) \tag{5}$$

where υ_p is the Poisson's ratio of the particle and β is a correction factor. A value of 1.05 for β was recommended by Oliver and Pharr [14] and used in this investigation.

It is evident that estimation of the projected contact area at the maximum indentation force is a key step in measuring the elastic modulus of the particle. Eq. (5) is strictly suitable only for measuring the elastic modulus of monolithic and isotropic specimens, and Eq. (3) is based strictly on the indentation phenomenon of sink-in, where the surface around the indenter is lower than the sample as a whole, as illustrated in Fig. 3a. In the case of sink-in, the contact depth h_c is always smaller than the maximum indentation depth $h_{\max}$, which is demonstrated by Eq. (3). When the Oliver–Pharr method is applied to probe the elastic modulus of the particle in a composite, as illustrated in Fig. 1, the difference of the matrix's properties might affect the measured result and pile-up (illustrated in Fig. 3b) might occur in such a system. These two issues are the

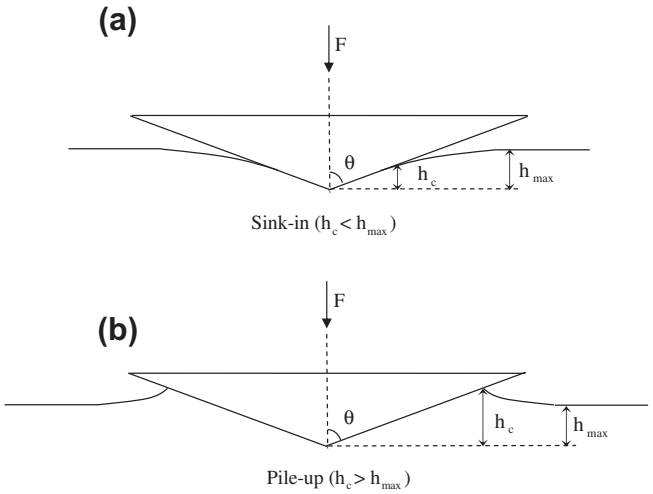

Fig. 3. Schematics of sink-in (a) and pile-up (b).

focus of our current investigation. Numerical results from our case studies are presented and discussed in the following section.

3. Results and discussion

3.1. A stiff particle embedded in a soft matrix

In the numerical simulation of the indentation test shown in Fig. 1 for our first case study, we chose a stiff particle embedded in a soft matrix. The material properties for the particle and the matrix are listed in Table 1, which corresponds to aluminium nitride (AlN) nanoparticles reinforced aluminium [8]. The radius of the particle was taken as 40 nm.

The virtual indentation tests were carried out at different maximum indentation depths, h_{max}. As in reality, the indentation force versus indentation depth curve can be obtained from every simulation and this curve was then applied to predict the elastic modulus of the particle by strictly following the Oliver–Pharr method, which was described in previous section. The solid line with filled triangle marks in Fig. 4 shows the predicted elastic modulus normalised by the input real particle's elastic modulus, E_p^m/E_p, as a function of the normalised maximum indentation depth, h_{max}/R. This can be compared to the dashed line, which represents the accurate value of the particle's elastic modulus, when $h_{max}/R \leq 0.02$, the predicted values E_p^m/E_p are very close to the ideal value of 1.0, with the error less than 10%. For greater indentation depths, the numerical curve decreases rapidly, indicating the increasing influence of the matrix with the increase in indentation depth. Due to the fact that the matrix has a much lower value of elastic modulus than that of the particle, the effect of the matrix leads to the decrease in the predicted indentation modulus.

Fig. 4 also shows that the predicted value by using the Oliver–Pharr method reaches a value even less than 0.21, which equals to the normalised matrix's modulus (see Table 1), when the normalised maximum indentation depth is over 0.225. This predicted result is clearly unacceptable. Further investigation indicates that such unacceptable results were due to the fact that Eqs (3) and (4) used to estimate the projected contact area in the Oliver–Pharr method is only suitable for the indentations where the surrounding matrix displays sink-in behaviour. As shown in Fig. 5, pile-up happens in the indentation for this case. Additionally, the particle has a large rigid body motion due to the large deformation of the matrix surrounding the particle and this contributes a large amount to the indentation depth. Due to these two facts, Eqs (3) and (4) cannot be applied to estimate the projected contact area with sufficient accuracy. In our finite element simulations, the projected contact area can, however, be obtained accurately from the numerical results. Fig. 6 shows the normalised predicted contact area from Eqs (3) and (4) as a function of the normalised maximum indentation depth, compared with the results obtained directly from the finite element simulations. It is evident that the prediction of the contact area from Eq. (4) is reliable only when $h_{max}/R \leq 0.08$. At greater depths, the error of the prediction increases with increase in indentation depth. It is worth mentioning that the projected indenter contact area under the maximum indentation force can be measured from imaging techniques, such as SEM and AFM, in a real physical test.

Table 1
The mechanical properties of the stiff particle and the soft matrix applied in Case One.

	Elastic modulus (GPa)	Poisson's ratio	Yield strength (MPa)
Particle	330	0.3	2100
Matrix	70	0.3	50

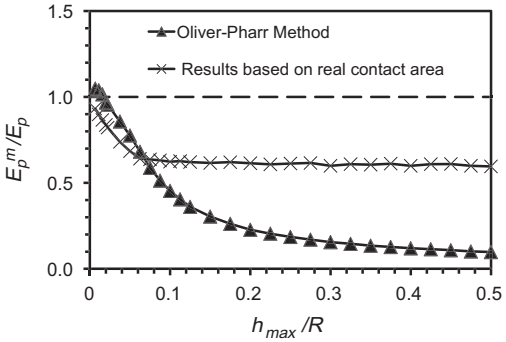

Fig. 4. Results of the probed elastic modulus of the particle as a function of the indentation depth for Case One.

Using the real contact area shown in Fig. 6, Eq. (5) was applied to predict the elastic modulus of the particle and the results were plotted in Fig. 4, marked by the "x" symbol. The value became constant for values of $h_{max}/R \geq 0.1$, still some 42% less than the actual input modulus value, which shows that the predicted elastic modulus from the indentation test by using the Oliver–Pharr method is a combined result that also involves the influence of the matrix.

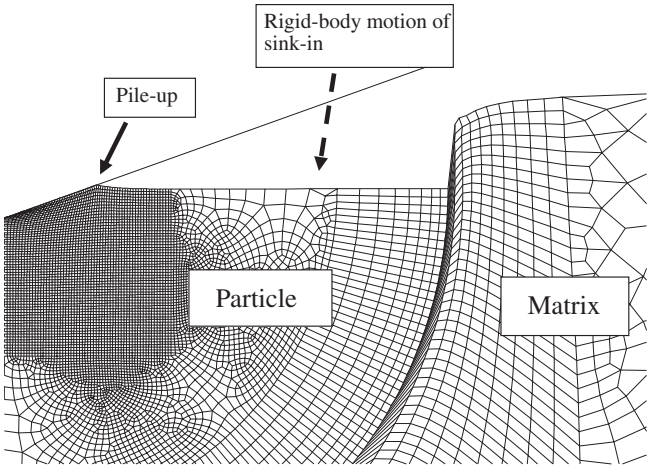

Fig. 5. Deformed particle and the surrounding matrix at the indentation depth of $h_{max}/R = 0.25$ for Case One, which shows local pile-up around the indenter and large rigid-body motion of sink-in of the particle.

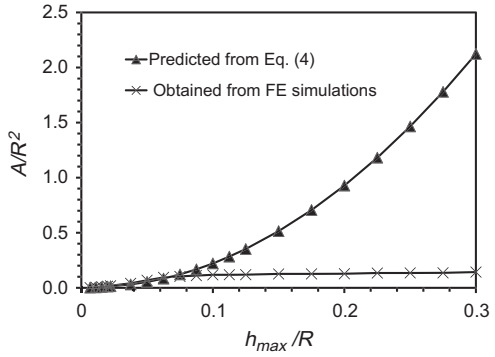

Fig. 6. The normalised predicted contact area as a function of the normalised maximum indentation depth from Eq. (4) for Case One, compared with the results obtained directly from the finite element simulations.

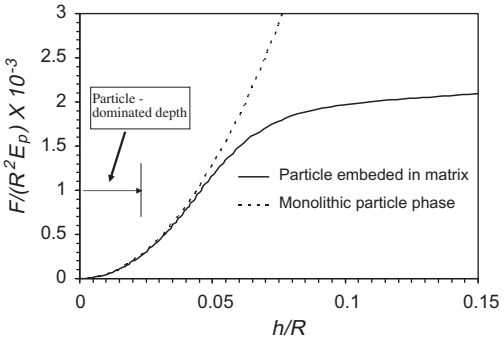

Fig. 8. Comparison of the indentation curves from the monolithic particle phase indentation and the composite indentation to confirm and to define the particle dominated depth for Case One.

Figs. 4 and 6 demonstrate that the influence of the matrix on the indentation can be negligibly small if the indentation depth is sufficiently small. Conversely, the influence of the matrix is significant if the indentation depth is reasonable large. This effect can also be observed from the indentation force versus indentation depth curve, as shown in Fig. 7. Referring to Figs. 4, 6 and 7, the indentation curve can be divided into a narrow particle-dominated depth and a major matrix-influenced depth. When the indentation depth is within the particle-dominated depth, the predicted indentation modulus is close to the elastic modulus of the particle and indentation method can still be applied to measure the particle's elastic modulus. According to Fig. 4, the particle dominated depth corresponds to values of $h_{max}/R \leq 0.02$. When the indentation depth is within the major matrix-influenced depth (where $h_{max}/R > 0.02$), the predicted indentation modulus can be significantly different from the particle's elastic modulus. In the current studied case, the difference can reach to 42% according to Fig. 4. Theoretically, the particle-dominated depth can be confirmed and defined by comparing the numerical indentation curves from both the monolithic particle phase indentation and the composite indentation experiments, and the comparison for this case is shown in Fig. 8. It confirms that the matrix starts to affect the indentation curve of the composite when $h_{max}/R > 0.02$ and thus the particle-dominated depth is $h_{max}/R \leq 0.02$. To effectively apply the indentation method to measure the elastic modulus of a particle embedded in a matrix in practice, it is important to understand the limits of the particle dominated-depth, so as to make sure that the indentation displacement remains within this depth. In the case of measurement of the elastic modulus of a thin film deposited on a substrate using an indentation method, the thin film-dominated depth is 10% of the film thickness [5,13].

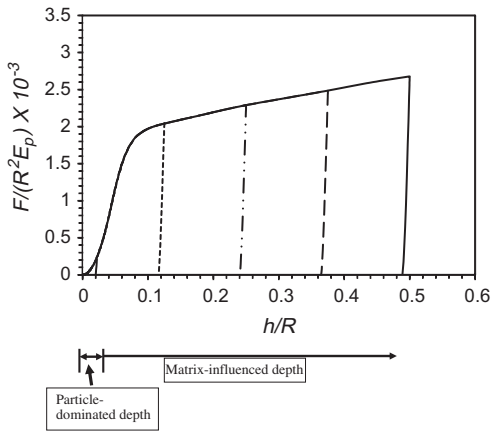

Fig. 7. Normalised indentation curve with unloading at different values of the maximum indentation depth, h_m for Case One. This curve can be divided into a narrow particle dominated depth and a major matrix influenced-depth.

3.2. A soft particle embedded in a stiff matrix

In our second case study, we chose a soft particle embedded in a stiff matrix. The material properties for the particle and the matrix are shown in Table 2, which corresponds in this example to graphite defects embedded in a cast iron [7]. The radius of the particle was taken as 40 μm.

Fig. 9 shows the deformed particle and the surrounding matrix at the indentation depth of $h_{max}/R = 0.25$. There exist double pile-ups of the soft particle material around the indenter and around the interface between the particle and the matrix, showing significantly different behaviour from Case One of a stiff particle embedded in a soft matrix. This deformation involving double pile-up is

Table 2
The mechanical properties of the soft particle and the stiff matrix applied in Case Two.

	Elastic modulus (GPa)	Poisson's ratio	Yield strength (MPa)
Particle	35	0.126	120
Matrix	210	0.29	300

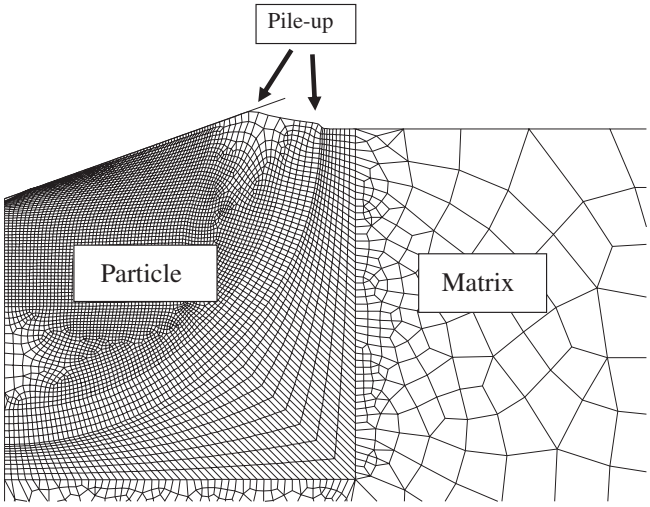

Fig. 9. Deformed particle and the surrounding matrix at the indentation depth of $h_{max}/R = 0.25$ for Case Two, which shows double pile-up of the soft particle material around the indenter and around the interface between the particle and the matrix.

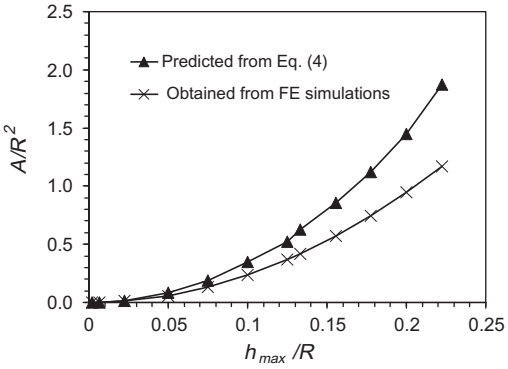

Fig. 10. The normalised predicted contact area as a function of the normalised maximum indentation depth from Eq. (4) for Case Two, compared with the results obtained directly from the finite element simulations.

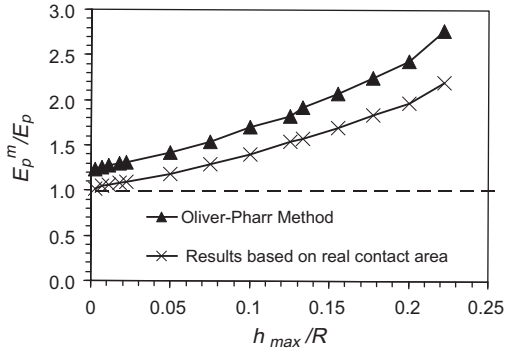

Fig. 11. Results of the probed elastic modulus of the particle as a function of the indentation depth for Case Two.

due to the different properties of the particle and the matrix. Further research is being carried out to investigate the origin and influences on this mode of deformation in some detail.

As expected, Eq. (3) will not be able to accurately estimate the contact depth and the projected contact area due to this different deformation morphology. Fig. 10 compares the predicted contact area from Eq. (4) with the real contact area obtained directly from the simulations. It confirms that the prediction of the contact area from Eq. (4) is only reliable when $h_{\max}/R$ is very small, and the error of the prediction increases with any increase of the indentation depth.

As for Case One, the elastic modulus of the soft particle was predicted by using the projected contact area from Eq. (4) and the real contact area obtained from the simulation, respectively and these predicted results are shown in Fig. 11. The results show that the predicted elastic modulus determined using the Oliver–Pharr method is always larger than that predicted from the real contact area, at different depths. The predicted values increase with the indentation depth continuously due to the influence of the stiff matrix. However, the most important finding from Fig. 11 is that there exists a particle-dominated depth and when $h_{\max}/R \leq 0.025$, the error of the predicted elastic modulus from the real contact area is less than 10%. Therefore, if the indentation depth is within the particle dominated depth, the Oliver–Pharr method can still be applied to predict the elastic modulus of the soft particle. Instead of using Eq. (4), the real contact area should be used in the prediction.

4. Summary

Finite element simulations were applied to investigate the indentation of particles embedded in composites and to validate the applicability of the Oliver–Pharr method to measure the elastic modulus of the particles. Two cases, a stiff particle and a soft particle, have been considered in this investigation. Our case study indicates that Oliver–Pharr method cannot be applied to accurately estimate the contact area due to complicated pile-up deformation. In addition, the real contact area is necessary to accurately determine the elastic modulus. Furthermore, in each case there exists a particle-dominated depth, and if the indentation depth is within this particle-dominated depth, the Oliver–Pharr method can still be applied to measure the particle's elastic modulus with sufficient accuracy, provided that the real contact area is used. In a true practical experimental sense the real contact area under the maximum indentation force for a sharp conical indenter can readily be obtained from imaging techniques, such as SEM and AFM. A parametric study is being carried out to understand the particle-dominated depth for different composite systems.

References

[1] Cheng YT, Cheng CM. Relationships between initial unloading slope, contact depth, and mechanical properties for spherical indentation in linear viscoelastic solids. Mater Sci Eng A 2005;409(1–2):93–9.
[2] Yan W, Sun Q, Feng XQ, Qian L. Determination of transformation stresses of shape memory alloy thin films: a method based on spherical indentation. Appl Phys Lett 2006;88:241912.
[3] Yan W, Sun Q, Liu HY. Spherical indentation hardness of shape memory alloys. Mater Sci Eng A 2006;425(1–2):278–85.
[4] He LH, Fujisawa N, Swain MV. Elastic modulus and stress–strain response of human enamel by nanoindentation. Biomaterials 2006;27(24):4388–98.
[5] Fischer-Cripps AC. Critical review of analysis and interpretation of nanoindentation test data. Surf Coat Technol 2006;200(14–15):4153–65.
[6] Yan W, Pun CL. Spherical indentation of metallic foams. Mater Sci Eng A 2010;527(13–14):3166–75.
[7] Pradhan SK, Nayak BB, Sahay SS, Mishra BK. Mechanical properties of graphite flakes and spherulites measured by nanoindentation. Carbon 2009;47(9):2290–2.
[8] Liu YQ, Cong HT, Wang W, Sun CH, Cheng HM. AlN nanoparticle-reinforced nanocrystalline Al matrix composites: fabrication and mechanical properties. Mater Sci Eng A 2009;505(1–2):151–6.
[9] Lee H, Mall S, He P, Shi DL, Narasimhadevara S, Yeo-Heung Y, et al. Characterization of carbon nanotube/nanofiber-reinforced polymer composites using an instrumented indentation technique. Composites: Part B – Eng 2007;38(1):58–65.
[10] Das B, Prasad KE, Ramamurty U, Rao CNR. Nano-indentation studies on polymer matrix composites reinforced by few-layer graphene. Nanotech 2009;20(12):125705.
[11] Oliver WC, Pharr GM. An improved technique for determining hardness and elastic modulus using load and displacement sensing indentation experiments. J Mater Res 1992;7(6):1564–83.
[12] Bolshakov A, Pharr GM. Influences of pile-up on the measurement of mechanical properties by load and depth sensing indentation techniques. J Mater Res 1998;13(4):1049–58.
[13] Hay JL, Pharr GM. Instrumented indentation testing. ASM handbook, vol. 8. Materials Park (OH): ASM International; 2000. p. 232–43.
[14] Oliver WC, Pharr GM. Measurement of hardness and elastic modulus by instrumented indentation: advances in understanding and refinements to methodology. J Mater Res 2004;19(1):3–20.